J Mol Model (2012) 18:2981–2991
DOI 10.1007/s00894-011-1316-9

ORIGINAL PAPER

Hydrogen adsorption capacities of multi-walled boron nitride nanotubes and nanotube arrays: a grand canonical Monte Carlo study

Zohreh Ahadi · Muhammad Shadman · Saeed Yeganegi · Farid Asgari

Received: 20 August 2011 / Accepted: 18 November 2011 / Published online: 8 December 2011

Abstract Hydrogen adsorption in multi-walled boron nitride nanotubes and their arrays was studied using grand canonical Monte Carlo simulation. The results show that hydrogen storage increases with tube diameter and the distance between the tubes in multi-walled boron nitride nanotube arrays. Also, triple-walled boron nitride nanotubes present the lowest level of hydrogen physisorption, double-walled boron nitride nanotubes adsorb hydrogen better when the diameter of the inner tube diameter is sufficiently large, and single-walled boron nitride nanotubes adsorb hydrogen well when the tube diameter is small enough. Boron nitride nanotube arrays adsorb hydrogen, but the percentage of adsorbed hydrogen (by weight) in boron nitride nanotube arrays is rather similar to that found in multi-walled boron nitride nanotubes. Also, when the Langmuir and Langmuir–Freundlich equations were fitted to the simulated data, it was found that multi-layer adsorptivity occurs more prominently as the number of walls and the tube diameter increase. However, in single-walled boron nitride nanotubes with a small diameter, the dominant mechanism is monolayer adsorptivity.

Z. Ahadi (✉) · F. Asgari
Department of Science and Engineering, Abhar branch,
Islamic Azad University,
Abhar, Iran
e-mail: Zohreh.Ahadi@gmail.com

M. Shadman
Department of Chemistry, Faculty of Science,
University of Zanjan,
P.O. Box 45195-313, Zanjan, Iran

S. Yeganegi
Department of Physical Chemistry, Faculty of Chemistry,
University of Mazandaran,
Babolsar, Iran

Keywords Boron nitride nanotubes · Grand canonical Monte Carlo · Adsorption · Storage · Hydrogen · Nanotube arrays

Introduction

Hydrogen storage is an important research field, as hydrogen storage is a prominent component of many industrial goals, and is of great interest to both scientists and investors for economic and environmental reasons [1]. Extensive studies that were ultimately aimed at efficient gas storage, especially hydrogen storage in nanostructures such as nanotubes, and which utilize either experimental or theoretical approaches have been performed [2–8]. In this research field, one of the most important considerations is the physisorption of hydrogen on and in carbon nanotubes (CNTs) and boron nitride nanotubes (BNNTs). So far, many researchers have focused their theoretical and experimental studies on various forms of CNTs in order to determine their storage capacities [9–11], although some papers have investigated hydrogen physisorption in single-walled boron nitride nanotubes [12, 13] and their arrays [14] using molecular simulation procedures.

In 2007, Cheng et al. simulated hydrogen storage in single-walled boron nitride nanotubes (SWBNNTs) [12] and single-walled boron nitride nanotube arrays (SWBNNTAs) [14] using a grand canonical Monte Carlo (GCMC) simulation program designed by them. They showed that SWBNNTs can adsorb more hydrogen than single-walled carbon nanotubes (SWCNTs) for the same nanotube chirality and under the same thermodynamic conditions. It should be noted that to achieve the same nanotube chirality, any BNNT must have a larger diameter than the equivalent CNT. Also, investigations of hydrogen physisorption in multi-walled boron nitride nanotubes (MWBNNTs) and their arrays (MWBNNTAs) have not

yet been done—all reported calculations in this field have attempted to estimate the hydrogen storage inside SWBNNTs and SWBNNTAs [12–14]. Note that the process of separating the SWBNNTs from the SWBNNTAs after producing them in special chemical reactions is far from simple. This means that pure SWBNNTs and pure SWBNNTAs are very expensive to produce and therefore use in industrial activities. Thus, it would be more economical to use MWBNNTs and MWBNNTAs as gas adsorbents, as they are easier to produce than SWBNNTs and SWBNNTAs. Such applications of nanotubes would enable a new system of delivering energy, called the "hydrogen economy" [1], as well as novel advanced interdisciplinary science associated with it. Therefore, studying and observing the abilities of MWBNNTs and MWBNNTAs to act as hydrogen adsorbents—as we have done in the work described in the present paper—can help us to determine whether they are good candidates for practical gas/hydrogen storage materials [12–16].

In this paper, we first provide a brief review of GCMC and the model employed in the simulation method that we utilized. We then present our results for hydrogen adsorption in MWBNNTs and MWBNNTAs, and compare these results with those obtained for hydrogen physisorption by SWBNNTs and SWCNTs. A conclusions section rounds off the paper.

The model used and the GCMC simulations performed

In this work, following an approach previously described in the literature [16–18], we used GCMC simulations to investigate hydrogen adsorption in SW/DW/TW BNNTs (SW=single-walled, DW=double-walled, TW=triple-walled) and arrays of them (SW/DW/TW BNNTAs). The diameters of the BNNTs considered are shown in Table 1. All BNNTs investigated were 4 nm in length. In this paper, the related notations used for the DWBNNTs and TWBNNTs are written as (m,m)@(n,n) and (m,m)@(n,n)@(k,k), respectively. In each case, the contents of the first set of parentheses relate to the innermost nanotube; the contents of the second set of parentheses relate to the middle nanotube, and (only in the case of TWBNNTs) the contents of the last set of parentheses relate to the outermost nanotube. For example, an (11,11)@(15,15) DWBNNT is a double-walled nanotube with an inner (11,11) nanotube and an outer (15,15) nanotube, while an (8,8)@(11,11)@(15,15) TWBNNT is a triple-walled nanotube with an innermost (8,8) nanotube, a middle (11,11) nanotube, and an outermost (15,15) nanotube. Furthermore, it should be noted that the major diameter of a DW/TW BNNT is equal to the diameter of its outermost nanotube, and only the diameter of the inner nanotube was varied for the DW/TW BNNTs examined in the simulations performed in this work. For example, (7,7)@(15,15)@(22,22) TWBNNTs and (15,15)@(22,22) and (7,7)@(22,22) DWBNNTs have the same major diameter—the diameter of a (22,22) SWBNNT, which is the outermost nanotube in all of these double- or triple-walled nanotubes.

In GCMC simulation, the configurations are sampled from a grand canonical (GC) ensemble, the temperature (T), volume (V), and chemical potential (μ) are kept constant during the simulation [16–18], and periodic boundary conditions (PBC) are applied at the open ends of the BNNTs during movements in the GCMC simulation until the number of hydrogen molecules in the simulation cell reaches equilibrium [16, 18]. In the actual molecular computations, the spherical cut-off distance was set to a little less than the half the simulation cell [16, 18].

In GCMC, for a fixed simulation cell, three types of moves are used to generate a Markov chain. These three types of operations are displacement (moving), creation, and deletion, which are performed with equal probability in order to add a hydrogen molecule inside the BNNT. The difference between the total potential energy before and after a creation operation must be calculated, and then, based on the assumed acceptance probabilities, this operation will either be accepted or not [13, 16–18]. In other words, after selecting a particle at a random position (r=initial position) and calculating the total potential energy of the system $U(r)$, the algorithm generates a random particle displacement (r'=final position) and calculates the new total potential energy of the system $U(r)$, and then accepts this particle displacement from its initial position to its final position with a probability of min[1, $\exp(-\Delta U/k_{\mathrm{B}}T)$], where $\Delta U = U(r) - U(r')$ [18]. In GCMC simulation, hydrogen–hydrogen, hydrogen–boron, and hydrogen–nitrogen interactions are considered based on the spherical Lennard–Jones (LJ) pair potential model, which can be described as follows [18]:

$$U(r_{ij}) = 4\varepsilon_{ij}\left[\left(\sigma_{ij}/r_{ij}\right)^{12} - \left(\sigma_{ij}/r_{ij}\right)^{6}\right], \quad (1)$$

where ε_{ij} and σ_{ij} are the energy and length parameters in the Lennard–Jones potential, and r_{ij} denotes the distance between the centers of particles i and j. In the simulation, the parameters ε_{ij} and σ_{ij} are the cross-interaction parameters, which are derived from the Lorentz–Berthelot mixing rules [16, 18]. Table 1 presents Lennard–Jones potential parameter values for hydrogen as a fluid and for boron and nitrogen as BNNT atoms.

In our GCMC simulation, each run consisted of 2.5×10^7 GCMC moves. The first 1.25×10^7 moves were considered to correspond to an equilibration period, and were thus discarded; only the final 1.25×10^7 moves were used to calculate ensemble averages of thermodynamic parameters. The multipurpose simulation code of a molecular simulation package was used for all simulations [17]. The BNNTs were

Table 1 Diameters of the SW/DW/TW BNNTs considered in this work

SWBNNT	Diameter (nm)	DWBNNT>*	DWBNNT<*	TWBNNT	Diameter (nm)
(7,7)	0.96	(11,11)@(15,15)	(8,8)@(15,15)	(8,8)@(11,11)@(15,15)	2.06
(8,8)	1.10	(15,15)@(22,22)	(7,7)@(22,22)	(7,7)@(15,15)@(22,22)	3.03
(10,10)	1.38	(19,19)@(29,29)	(10,10)@(29,29)	(10,10)@(19,19)@(29,29)	3.99
(11,11)	1.51	(29,29)@(44,44)	(15,15)@(44,44)	(15,15)@(29,29)@(44,44)	6.05
(15,15)	2.06	(39,39)@(58,58)	(19,19)@(58,58)	(19,19)@(39,39)@(58,58)	7.98
(19,19)	2.61	(48,48)@(73,73)	(24,24)@(73,73)	(24,24)@(48,48)@(73,73)	10.04
(22,22)	3.03				
(24,24)	3.30	LJ parameter	Hydrogen [12]	B (nanotube) [12]	N (nanotube) [12]
(29,29)	3.99	σ (nm)	0.2958	0.3453	0.3365
(39,39)	5.36	ε/k_B (K) **	36.7	47.8	72.9
(44,44)	6.05	LJ parameter	Carbon [12]		
(48,48)	6.60	σ (nm)	0.34		
(58,58)	7.98	ε/k_B (K)	28.2		
(73,73)	10.04				

* *DWBNNT*> indicates a DWBNNT where the diameter of the inner nanotube is relatively large compared to (although, of course, still smaller than) the major diameter of the DWBNNT, while *DWBNNT*< indicates a DWBNNT where the diameter of the inner nanotube is relatively small compared to the major diameter

** k_B is the Boltzmann constant

assumed to have rigid structures, and no changes in the geometry of the adsorbent (i.e., BNNT here) were considered, since the changes to the geometries of BNNTs that are induced by hydrogen molecules at room temperature can be neglected. Finally, the isotherms for the adsorption of hydrogen by SW/DW/TW BNNTs and SW/DW/TW BNNTAs that are plotted in the next section correspond to 293 K.

Results and discussion

After running simulations and obtaining data using GCMC calculations, we were able to plot the adsorption isotherms for hydrogen inside MWBNNTs and MWBNNTAs. We first considered two SWBNNTs [(15,15) and (22,22)], four DWBNNTS [(8,8)@(15,15); (11,11)@(15,15); (7,7)@(22,22); and (15,15)@(22,22)] and two TWBNNTs [(8,8)@(11,11)@(15,15) and (7,7)@(15,15)@(22,22)] at 293 K. Fixing the tube length and varying the pressure, we plotted the percentage by weight of adsorbed hydrogen (H_2/system wt%) against pressure; the results can be seen in Fig. 1a. This figure shows that the hydrogen loading inside the BNNTs increases as a function of pressure.

As the pressure of hydrogen increases, the hydrogen loading increases. However, the percentage by weight of adsorbed hydrogen increases more rapidly within SWBNNTs, and hydrogen storage decreases with the number of nanotube walls; in other words, (15,15) and (22,22) SWBNNTs show enhanced hydrogen physisorption compared to that of (8,8)@(11,11)@(15,15) and (7,7)@(15,15)@(22,22) TWBNNTs under the same thermodynamic conditions. The results also show that the TWBNNTs all have similar hydrogen storage values, while more variation in the hydrogen storage values is observed for the SWBNNTs. From Fig. 1a, it is clear that the percentages by weight of adsorbed hydrogen in DWBNNTs lie between those of SWBNNTs and TWBNNTs. In fact, for large-diameter DWBNNTs with a relatively narrow internal nanotube [i.e., (7,7)@(22,22) DWBNNTs but not (15,15)@(22,22) DWBNNTs], the percentage by weight of adsorbed hydrogen is considerably higher than the corresponding values for the other DWBNNTs [those with a relatively wide internal nanotube; i.e, (15,15)@(22,22) DWBNNTs but not (7,7)@(22,22) DWBNNTs], which exhibit hydrogen adsorptivities between those of SWBNNTs and TWBNNTs. This result can be explained by noting that less hydrogen can be loaded into a narrow internal nanotube than into a wide internal nanotube. In other words, the interior space of the tube is an important factor in hydrogen physisorption by the BNNTs: DWBNNTs with a large major diameter show enhanced hydrogen adsorptivity, while DWBNNTs with a small major diameter can only adsorb hydrogen at low loadings due to reduced internal space.

Next, we compared the hydrogen adsorption isotherms for SWBNNTs and SWCNTs at 293K obtained based on our simulations and the results reported in [12]. Figure 1b presents this comparison. In [12], hydrogen physisorption by (15,15) and (22,22) SWBNNTs and SWCNTs at 293 K is reported, and our GCMC calculations for the same nanotubes and same thermodynamic conditions as used in [12] are presented in Fig. 1b. We found that the hydrogen

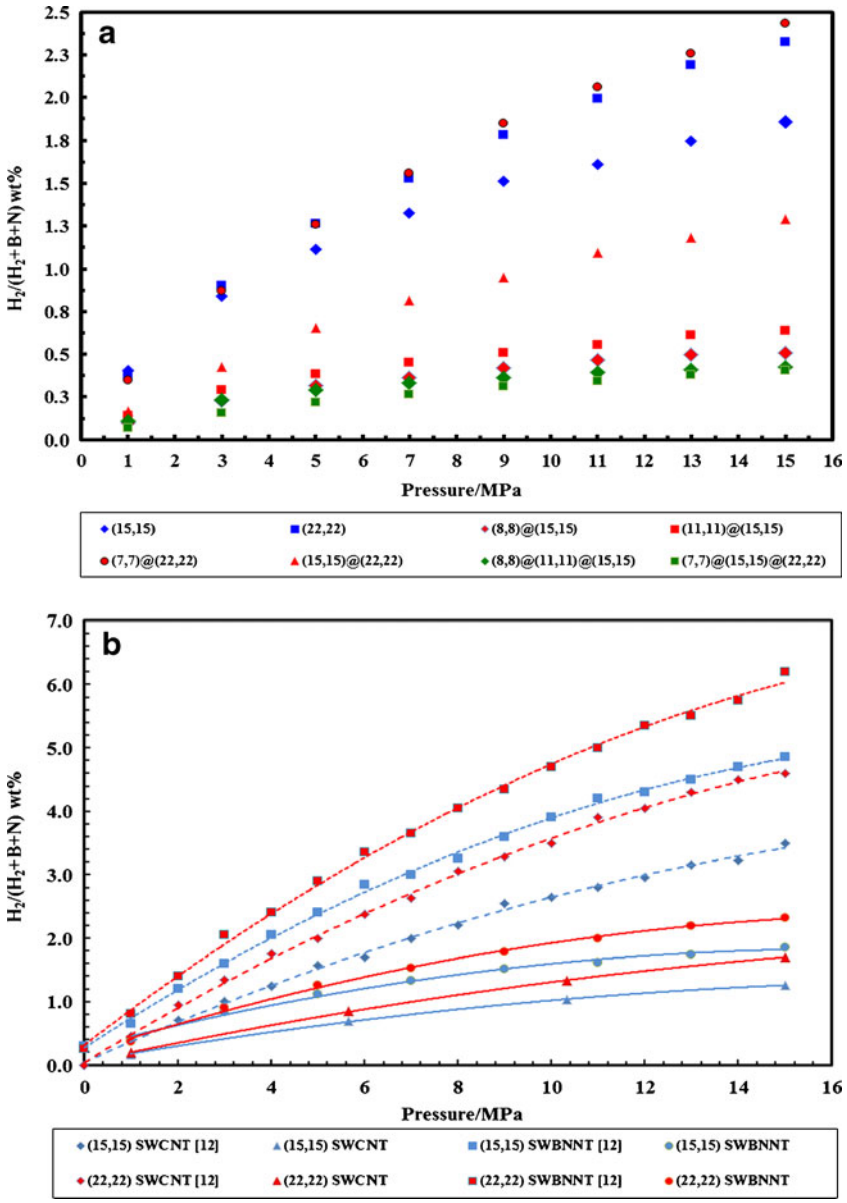

Fig. 1 **a** Isotherms of hydrogen physisorption in SW/DW/TW BNNTs at 293 K. **b** Comparison of the isotherms of hydrogen physisorption in SWBNNTs and SWCNTs at 293 K based on our data and the results in [12]. The *lines* correspond to second-order polynomial fits

physisorption data values from [12] are a little higher than the corresponding data values obtained from our calculations. It should be noted that we have performed our simulations using the multipurpose simulation code of Snurr's research group at Northwestern University [17]. Many articles have already been published that have made use of this simulation package [16, 19–21]. However, the hydrogen adsorption function behaves in the same manner in both the data from [12] and our reported data.

We calculated the Langmuir and Langmuir–Freundlich equation parameters for hydrogen adsorption via Eqs. 2 and 3 (below), respectively [16]:

$$\theta = \frac{Z}{Z_{\max}} = \frac{KP}{1+KP} \tag{2}$$

$$\theta = \frac{Z}{Z_{\max}} = \frac{AP^n}{1+AP^n}, \tag{3}$$

where θ is the fraction of the adsorbent's surface (BNNTs here) covered by the adsorbate (hydrogen here), P is the partial pressure of hydrogen, and $Z_{\max}$ (mol/m^3) is the maximum hydrogen loading (corresponding to complete coverage of the surface of the BNNT by hydrogen), while K [in (kPa)$^{-1}$], n, and A [the size of which is related to the value of n and is on the order of (kPa)$^{-1}$] are constants.

In this work, we investigated the adsorption of hydrogen inside BNNTs mathematically, comparing the results obtained using the Langmuir (L) and the Langmuir–Freundlich (L-F) equations. These equations can help us to find the best fit to the hydrogen physisorption data for illustrating the mathematical form of the adsorption, and the mechanism of

hydrogen physisorption (by comparing the equations). For the single-walled nanotubes, the Langmuir equation fitted well to the sorption data, meaning that hydrogen can be adsorbed as a monolayer inside the BNNTs. This can occur when the nanotube diameter is less than about 20 Å and the molecular gases can be adsorbed in a thermodynamically stable monolayer [16]. Thus, the Langmuir equation corresponds to monolayer gas sorption, while the Langmuir–Freundlich equation corresponds to multi-layer gas sorption in single-walled nanotubes. The grand canonical ensemble helps us to achieve this goal. However, the mechanism of hydrogen adsorption inside MWBNNTs is rather complicated. Figure 2a presents Langmuir and Langmuir–Freundlich equations fitted to the hydrogen sorption data for (15,15) and (22,22) SWBNNTs, and Fig. 2b shows cross-sections of these SWBNNTs with hydrogen adsorbed at 293 K and pressures of 1–15 MPa.

Figure 3a presents fits of the Langmuir and Langmuir–Freundlich equations to the hydrogen adsorption data for (8,8)@(15,15), (11,11)@(15,15), (7,7)@(22,22), and (15,15)@(22,22) DWBNNTs, while Fig. 3b shows cross-sections of these four DWBNNTs with hydrogen adsorbed onto them at 293 K and pressures of 1–15 MPa. Similarly, Fig. 4a depicts fits of the Langmuir and Langmuir–Freundlich equations to the hydrogen adsorption data for (8,8)@(11,11)@(15,15) and (7,7)@(15,15)@(22,22) TWBNNTs, while Fig. 4b shows cross-sections of these TWBNNTs with hydrogen adsorbed onto them at 293 K and pressures of 1–15 MPa.

In Figs. 2a, 3a, and 4a, we can see that the Langmuir–Freundlich equation gives the best fit to the adsorption data.

From Fig. 2a, it is clear that both the Langmuir equation and the Langmuir–Freundlich equation can be fitted to the data for both (15,15) and (22,22) SWBNNTs, and these two SWBNNTs show similar adsorptivity behavior. The fits to the data indicate that the mechanism of hydrogen physisorption in both (15,15) and (22,22) SWBNNTs is not monolayer adsorption; at least two layers of hydrogen can be adsorbed inside (15,15) and (22,22) SWBNNTs. This behavior can be observed in the cross-sections of the (15,15) and (22,22) SWBNNTs presented in Fig. 2b. According to results we reported previously, the adsorption of the second layer of gas inside a nanotube with a diameter of <2 nm is thermodynamically unstable [16]. Note that the diameters of the (15,15) and (22,22) SWBNNTs are 2.06 and 3.03 nm,

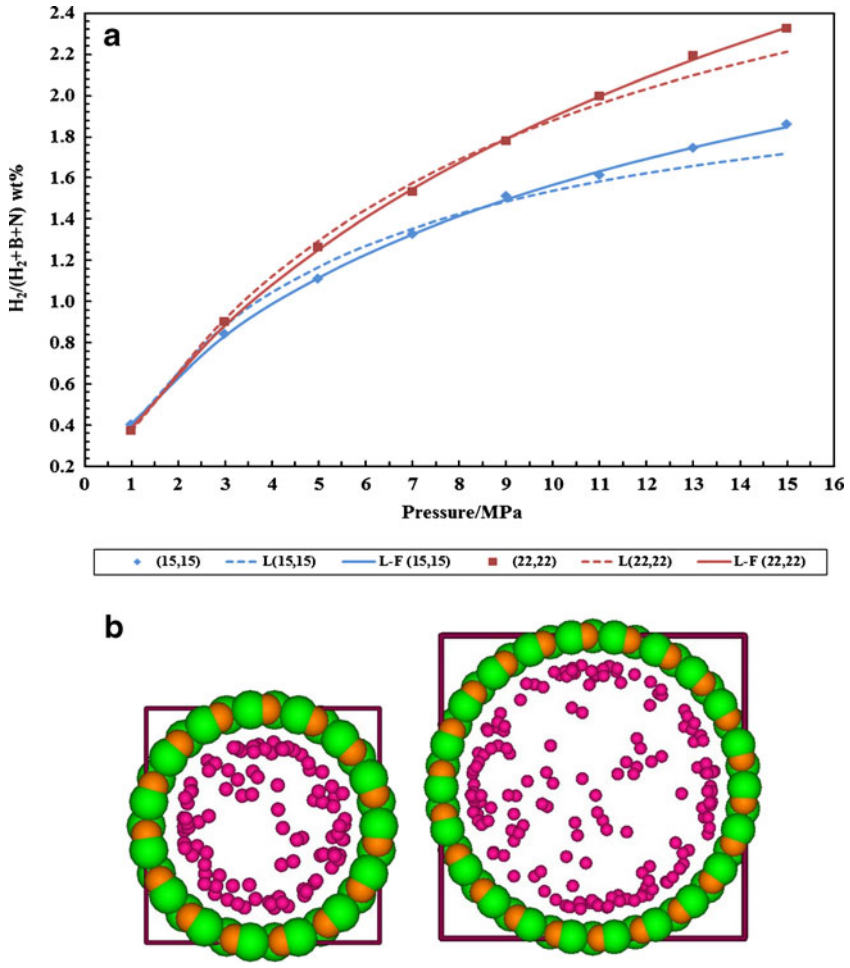

Fig. 2 **a** Isotherms of hydrogen physisorption in (15,15) and (22,22) SWBNNTs at 293 K. The *dashed lines* correspond to Langmuir fits and the *solid lines* correspond to Langmuir–Freundlich fits to the pressure. **b** Cross-sections of a (15,15) SWBNNT (*left*) and a (22,22) SWBNNT (*right*) that have been filled with hydrogen at 15 MPa and 293 K

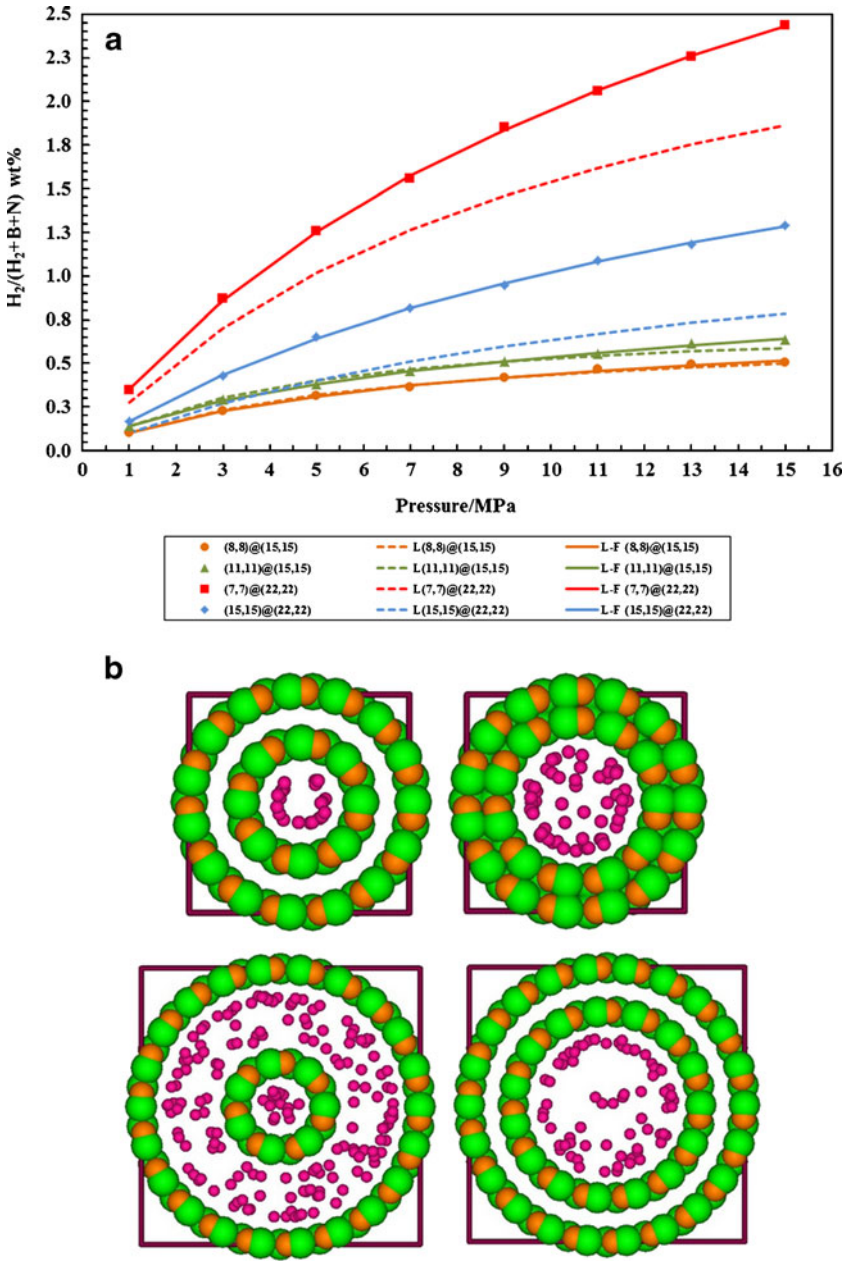

Fig. 3 **a** Adsorption isotherms for hydrogen physisorption by (8,8)@(15,15), (11,11)@(15,15), (7,7)@(22,22), and (15,15)@(22,22) DWBNNTs at 293 K. The *dashed lines* represent Langmuir fits and the *solid lines* show the Langmuir–Freundlich fits with pressure. **b** Cross-sections of an (8,8)@(15,15) DWBNNT (*top left*) and an (11,11)@(15,15) DWBNNT (*top right*), and cross-sections of a (7,7)@(22,22) DWBNNT (*bottom left*) and a (15,15)@(22,22) DWBNNT (*bottom right*) filled with hydrogen at 15 MPa and 293 K

respectively; thus, the probability of two-layer hydrogen adsorption in these nanotubes increases at high pressure.

Figure 3a illustrates that the Langmuir–Freundlich equation leads to a better fit to the hydrogen adsorptivity data than the Langmuir equation for the (7,7)@(22,22) and (15,15)@(22,22) DWBNNTs in particular. The figure also shows that the Langmuir–Freundlich and Langmuir equations provide similarly good fits to the data for the (8,8)@(15,15) and (11,11)@(15,15) DWBNNTs. It should be noted that the diameters of the (8,8)@(15,15) and the (11,11)@(15,15) DWBNNTs are both 2.06 nm, but the narrower inner nanotube reduces the space available for hydrogen storage in the former DWBNNT. Thus, monolayer adsorption of hydrogen occurs in DWBNNTs with diameters of less than about 2 nm, while DWBNNTs with diameters of more than 2 nm can adsorb hydrogen in two layers. Figure 3b shows cross-sections of (8,8)@(15,15) and (11,11)@(15,15) DWBNNTs with hydrogen adsorbed inside the nanotubes. For (11,11)@(15,15) DWBNNTs, when the pressure increases, hydrogen physisorption increases too; at high pressure, the data deviates from the Langmuir fit, indicating that (11,11)@(15,15) DWBNNTs can adsorb hydrogen in a second layer at high pressure—as observed in Fig. 3b. Figure 3b also shows that multi-layer hydrogen adsorption occurs for (7,7)@(22,22) and (15,15)@(22,22) DWBNNTs, leading to a good fit of the Langmuir–Freundlich equation to the data obtained from GCMC simulations of these DWBNNTs.

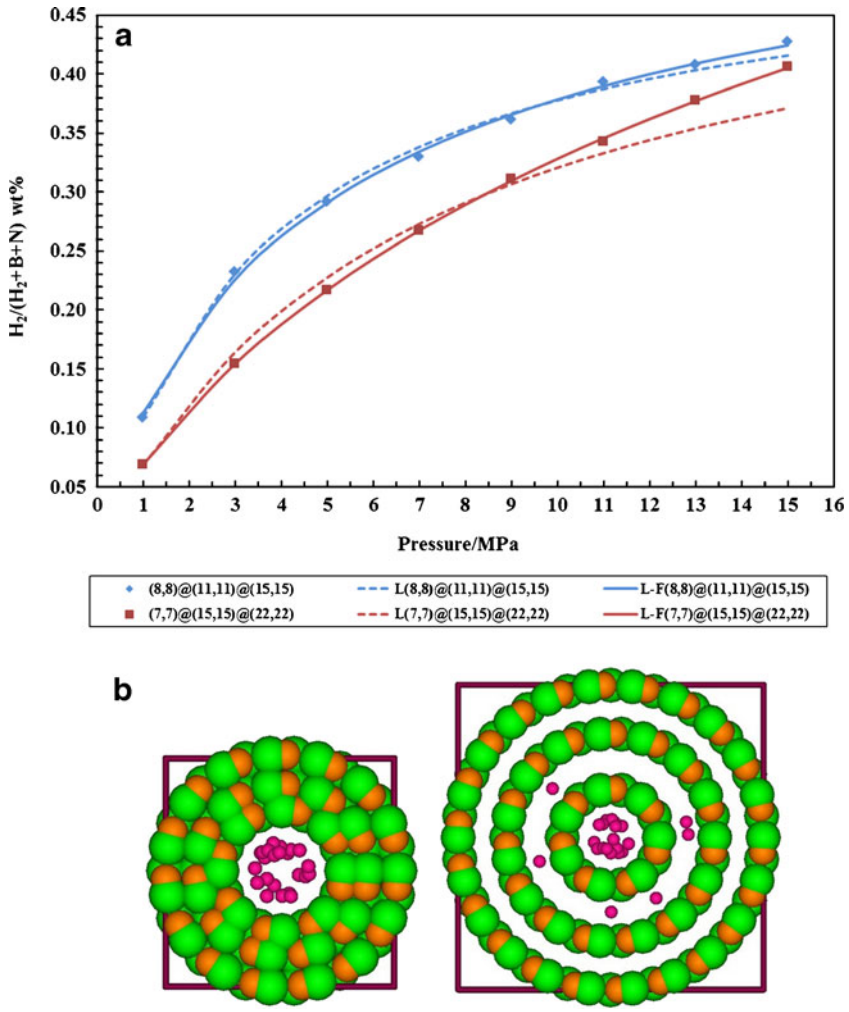

Fig. 4 **a** Isotherms for hydrogen physisorption by (8,8)@(11,11)@(15,15) and (7,7)@(15,15)@(22,22) TWBNNTs at 293 K. The *dashed lines* represent the Langmuir fits and the *solid lines* show the Langmuir–Freundlich fits with pressure. **b** Cross-sections of an (8,8)@(11,11)@(15,15) TWBNNT (*left*) and a (7,7)@(15,15)@(22,22) TWBNNT (*right*) that are filled with hydrogen at 15 MPa and 293 K

Figure 4a shows the fits of the Langmuir–Freundlich and the Langmuir equations to TWBNNTs. We can see that (8,8)@(11,11)@(15,15) TWBNNTs adsorb more hydrogen than (7,7)@(15,15)@(22,22) TWBNNTs. The diameter of an (8,8)@(11,11)@(15,15) TWBNNT is about 2.06 nm, while a (7,7)@(15,15)@(22,22) TWBNNT has a diameter of 3.03 nm. The reason that more hydrogen is adsorbed inside an (8,8)@(11,11)@(15,15) TWBNNT than inside a (7,7)@(15,15)@(22,22) TWBNNT is that there is a wider interior space inside an (8,8)@(11,11)@(15,15) TWBNNT. Although a (7,7)@(15,15)@(22,22) TWBNNT does have more widely spaced internal nanotube walls than an (8,8)@(11,11)@(15,15) TWBNNT, the spaces between the internal nanotube walls in a (7,7)@(15,15)@(22,22) TWBNNT are still relatively cramped, so intermolecular repulsion between the atoms of the internal nanotube walls as well as between those atoms and the adsorbed hydrogen is high, which in turn suppresses the adsorption of hydrogen in these spaces. Therefore, we would expect monolayer adsorption inside both (8,8)@(11,11)@(15,15) and (7,7)@(15,15)@(22,22) TWBNNTs. Figure 4a suggests that only hydrogen monolayer adsorption occurs inside both the (7,7)@(15,15)@(22,22) and (8,8)@(11,11)@(15,15) TWBNNTs up to a pressure of around 10 MPa; however, above this pressure, the adsorption data for the (7,7)@(15,15)@(22,22) TWBNNTs deviate from the Langmuir fit, indicating that hydrogen is being stored in a second layer. This is also shown in Fig. 4b, which depicts cross-sections of these TWBNNTs at 15 MPa and 293 K; at this pressure, the (7,7)@(15,15)@(22,22) TWBNNTs adsorb a second layer of hydrogen internally.

We now turn our attention to the effect of nanotube diameter on hydrogen adsorption. Figure 5a shows the percentage by weight of adsorbed hydrogen plotted as adsorption isotherms for SW/DW/TW BNNTs against nanotube diameter at 10 MPa and 293 K. In Fig. 5a, we can see that hydrogen adsorption increases as a function of nanotube diameter in all SW/DW/TW BNNTs. Also, according to this figure, SWBNNTs can adsorb more hydrogen than DW/TW BNNTs; DWBNNTs with a thin inner nanotube (DWBNNTs<) adsorb more hydrogen than DWBNNTs with a wide inner

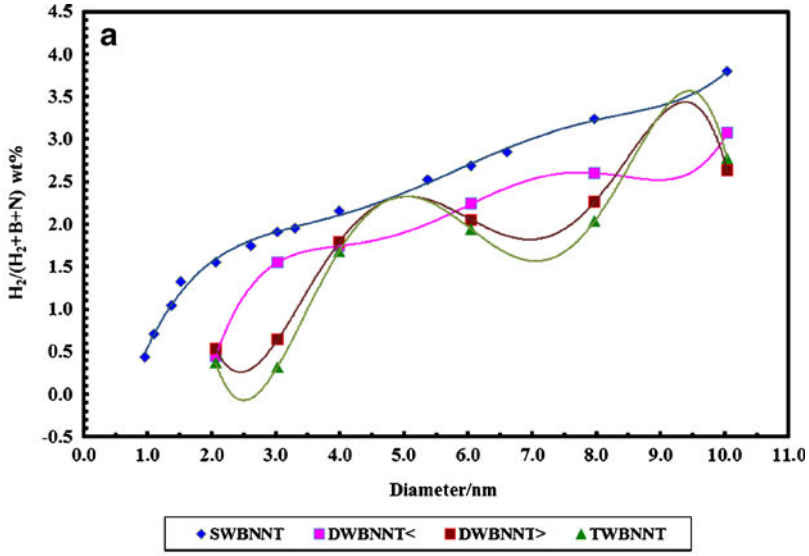

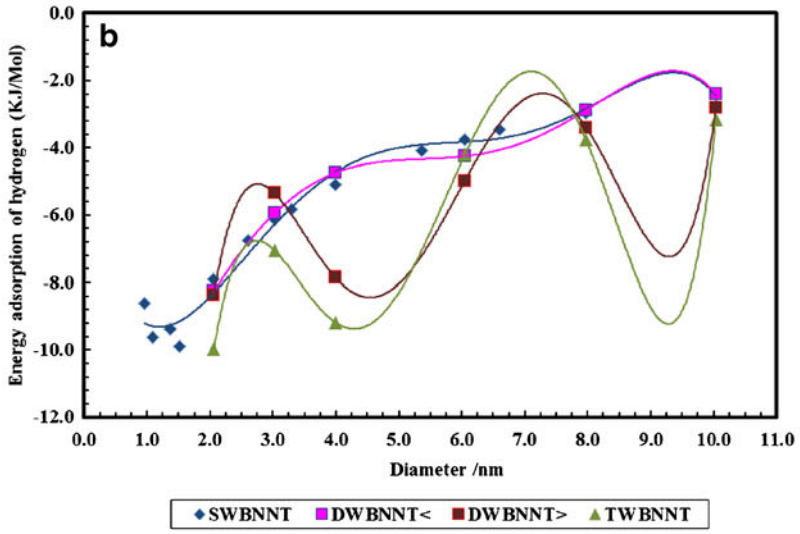

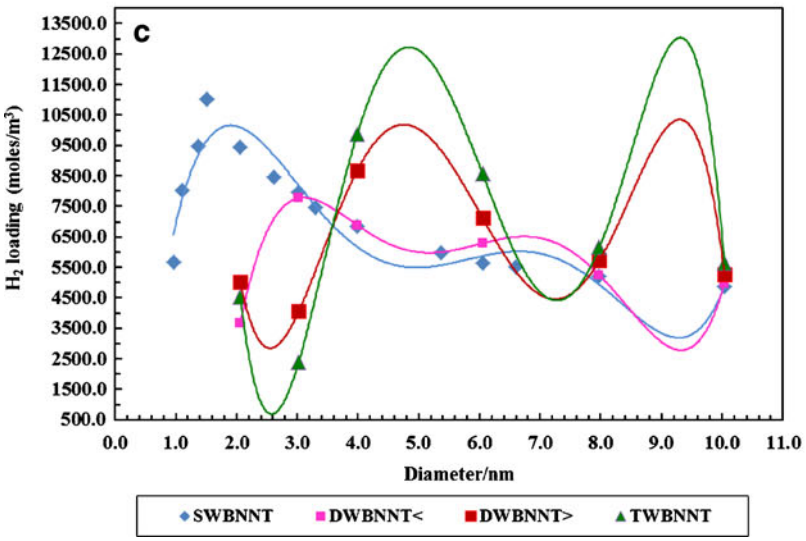

Fig. 5 **a** Hydrogen adsorption isotherms correspond to the unit of "the weight percentage of hydrogen adsorption" for SW/DW/TW BNNTs plotted against nanotube diameter at 10 MPa and 293K. **b** Energy of hydrogen adsorption for SW/DW/TW BNNTs plotted against nanotube diameter at 293 K. **c** Hydrogen adsorption isotherms correspond to the unit of "moles/m^3" for SW/DW/TW BNNTs plotted against nanotube diameter at 10 MPa and 293K

nanotube (DWBNNTs>); and TWBNNTs adsorb a similar wt % of hydrogen to DWBNNTs>. However, it is important to combine these results with those obtained from the GCMC simulation for the energy of hydrogen adsorption. Figure 5b presents plots of the energy of hydrogen adsorption by SW/DW/TW BNNTs versus nanotube diameter at 10 MPa and 293 K. The plots show that SWBNNTs and DWBNNTs<exhibit the same behavior of the energy of hydrogen adsorption with nanotube diameter, while DWBNNTs>and TWBNNTs also show similar behavior. It is also clear that, for each type of BNNT, the behavior seen in Fig. 5a is the opposite to that seen in Fig. 5b. To investigate this further, we replotted the hydrogen adsorption isotherms in another unit of hydrogen adsorption: mol/m^3; see Fig. 5c. Note that the data in Fig. 5c correlate well with the data in Fig. 5b. Figure 5c shows that hydrogen adsorption decreases with nanotube diameter, so the energy of hydrogen adsorption must decrease (the absolute value of the adsorption energy decreases), as seen in Fig. 5b. In Fig. 5c we also see that the SWBNNTs and DWBNNTs< have similar hydrogen storage capacities, and the same is true of DWBNNTs>and TWBNNTs; both of these results are also apparent in Fig. 5b. Therefore, according to Fig. 5b and c, increasing the nanotube diameter decreases hydrogen adsorption, and SWBNNTs can adsorb more hydrogen than other DW/TW BNNTs. However, the important result is that the most accurate unit of hydrogen adsorptivity is mol/m^3. Therefore, in order to perform the best comparison of the hydrogen adsorptivities of SW/DW/TW BNNTs, the units of adsorptivity must be converted into mol/m^3, but when we focus on a specific type of nanotube, it is not necessary to change from using percentage by weight of adsorbed hydrogen as a unit.

In our final investigation, we concentrated on hydrogen adsorption in SW/DW/TW BNNT arrays (SW/DW/TWBNNTAs). We calculated the distance between tubes (DBTs) based on the perpendicular distance between the surfaces of the outermost tubes of the BNNTs. Technically, the distance between two parallel nanotubes is the perpendicular distance between the major axes of the nanotubes. However, if we are investigating parallel nanotubes at various separations from each other, we can consider the DBT to be the perpendicular distance between the outer surfaces of the nanotubes, because the diameters of the nanotubes remain constant (and can therefore be neglected).

Figure 6a presents the percentage by weight of adsorbed hydrogen in SW/DW/TWBNNTAs at various DBTs from 1.09 to 1.39 Å (and at 10 MPa and 293 K). Figure 6a shows that hydrogen adsorption both inside and outside the SWBNNTAs increases with DBT and nanotube diameter. The difference between the percentages by weight of adsorbed hydrogen at a high DBT of 1.39 Å and a low DBT of 1.09 Å (at fixed nanotube diameter) is considerable for SWBNNTAs, while this difference is smaller for DWBNNTAs and smallest for TWBNNTAs. Figure 6b presents cross-sections of BNNTAs that have been filled with hydrogen at 10 MPa and 293 K. The cross-sections of four (7,7)@(15,15)@(22,22) TWBNNTAs where DBT=1.09 Å and 1.39 Å are shown top left and top right, respectively. The cross-sections of four (7,7)@ (22,22) DWBNNTAs where DBT=1.09 Å and 1.39 Å are shown center left and center right, respectively. Finally, the cross-sections of four (22,22) SWBNNTAs where DBT=1.09 Å and 1.39 Å are shown at the bottom left and bottom right of Fig. 6b, respectively. Based on Fig. 6b, we can conclude that more hydrogen is adsorbed in the interstitial space (the space between nanotubes) than inside the nanotubes (the internal spaces of the nanotubes). Note that the internal space of a nanotube is always fixed, because the diameter of a nanotube is always fixed. While a nanotube can adsorb a certain amount of hydrogen, varying the DBT changes the interstitial space, which in turn changes the amount of hydrogen adsorbed in this space. Figure 6b clearly shows that the hydrogen adsorbed in the internal spaces of the nanotubes under the same thermodynamic conditions remains almost the same for different DBTs, but the hydrogen that is physisorbed in the interstitial space increases with the DBT. However, the radial distribution function (RDF) of hydrogen must be calculated separately for the interstitial and interior spaces of the nanotubes using molecular dynamics (MD) in order to check that the presence of hydrogen outside the tubes is desirable.

Also, if we consider the data shown in Figs. 1a and 6a, we can see that the percentages by weight of adsorbed hydrogen in BNNTAs and BNNTs are fairly similar. Industrially synthesizing and separating out BNNTs is more difficult than it is for BNNTAs, which suggests that BNNTAs are better candidates than BNNTs for hydrogen adsorption materials.

Conclusions

In this work, we investigated the hydrogen adsorption of SW/DW/TW BNNTs and SW/DW/TW BNNTAs using GCMC simulation. We also investigated the mechanism of hydrogen adsorption by fitting the Langmuir and Langmuir–Freundlich equations to the hydrogen adsorption data. The results show that hydrogen adsorption increases with tube diameter and the distance between the tubes (when they are in arrays). TWBNNTs exhibited the lowest levels of hydrogen adsorption; this is because of the existence of atomic repulsion between hydrogen atoms and between hydrogen and nanotube atoms in TWBNNTs containing adsorbed hydrogen, which in turn is due to space constraints inside the TWBNNTs compared to the SW/DWBNNTs. When the inner tube diameter is sufficiently large, DWBNNTs can adsorb relatively large amounts of hydrogen, but SWBNNTs adsorb more hydrogen when the tube diameter is relatively small. The percentage by weight of hydrogen adsorbed by

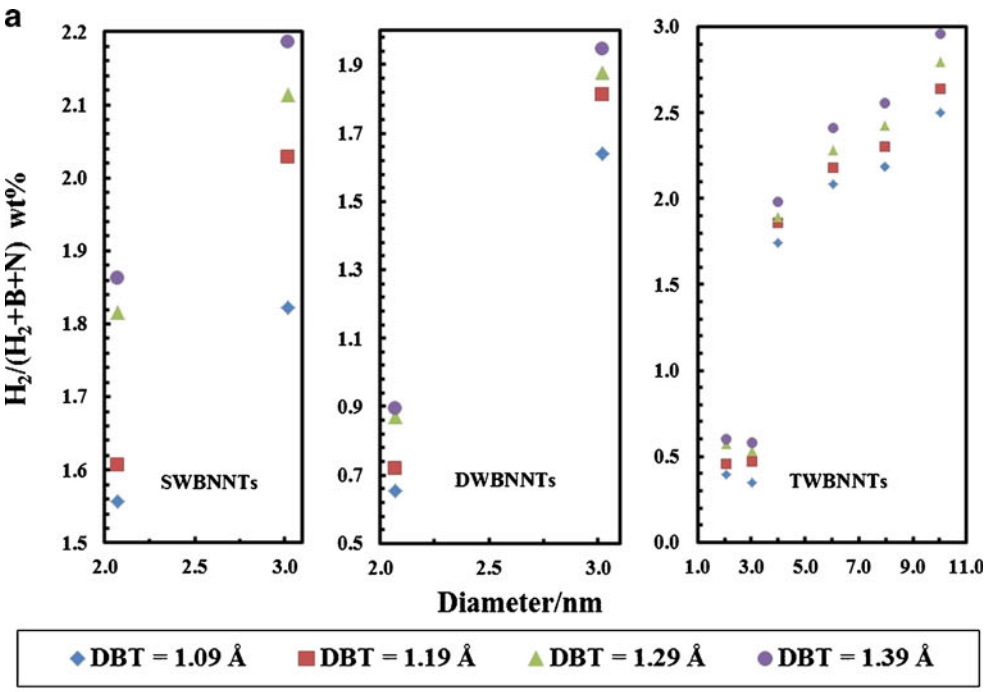

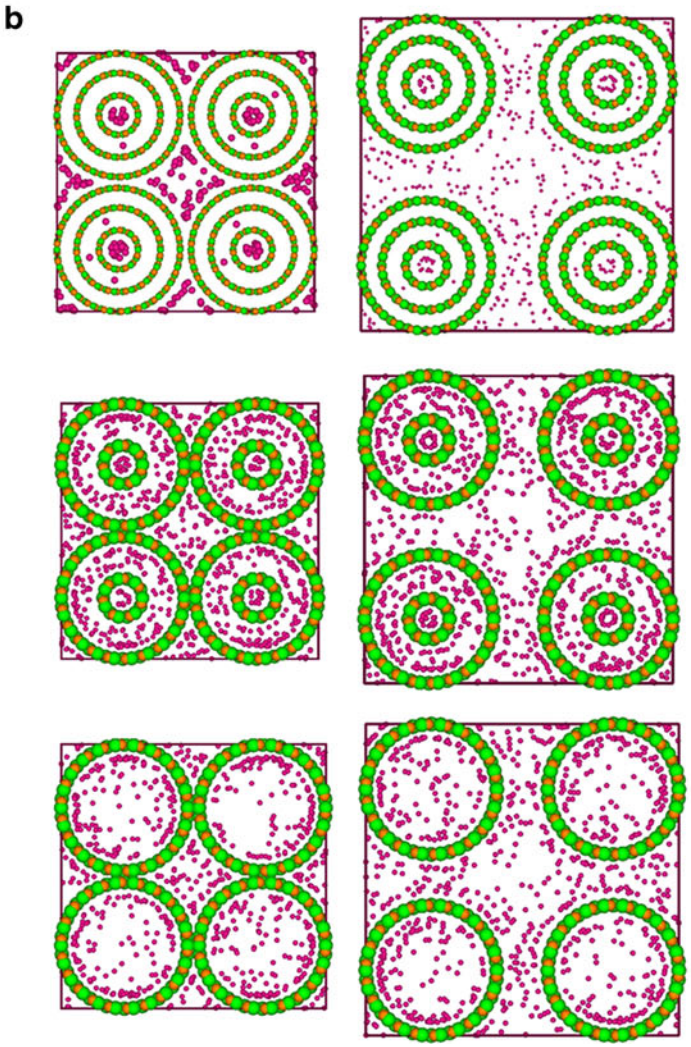

Fig. 6 **a** Isotherms of hydrogen physisorption in SW/DW/TW BNNTAs at different DBTs from 1.09 to 1.39 Å (at 10 MPa and 293 K). **b** Cross-sections of four (7,7)@(15,15)@(22,22) TWBNNTAs where the DBT= 1.09 Å (*top left*) and 1.39 Å (*top right*), respectively. Cross-sections of four (7,7)@(22,22) DWBNNTAs where DBT=1.09 Å (*center left*) and 1.39 Å (*center right*), respectively. Cross-sections of four (22,22) SWBNNTAs where DBT=1.09 Å (*bottom left*) and 1.39 Å (*bottom right*), respectively. These BNNTAs were filled with hydrogen at 10 MPa and 293 K

BNNTAs is similar to that adsorbed by BNNTs, which implies that BNNTAs are better candidates for hydrogen adsorption materials, as they are easier to industrially synthesize and separate than BNNTs. We also found that using units of mol/m^3 instead of the percentage by weight when comparing the adsorptivities of a series of nanotubes (of the same type) allows a better comparison. Finally, when we fitted the Langmuir and Langmuir–Freundlich equations to the simulation data, we noted that there is a trend towards multi-layer adsorptivity as the number of walls and the tube diameter are increased. However, in small-diameter SWBNNTs, the dominant mechanism is monolayer adsorption of hydrogen.

Acknowledgments We acknowledge the Abhar branch of the Islamic Azad University Research Council for its support of this work.

References

1. Sahaym U, Norton MG (2008) Advances in the application of nanotechnology in enabling a "hydrogen economy." J Mater Sci 43:5395–5429. doi:10.1007/s10853-008-2749-0
2. Lan J, Cheng D, Cao D, Wang W (2008) Silicon nanotube as a promising candidate for hydrogen storage: from the first principle calculations to grand canonical Monte Carlo simulations. J Phys Chem C 112:5598–5604. doi:10.1021/jp711754h
3. Kowalczyk P, Gauden PA, Terzyk AP (2008) Cryogenic separation of hydrogen isotopes in single-walled carbon and boron-nitride nanotubes: insight into the mechanism of equilibrium quantum sieving in quasi-one-dimensional pores. J Phys Chem B 112:8275–8284. doi:10.1021/jp800735k
4. Singh AK, Lu J, Aga RS, Yakobson BI (2011) Hydrogen storage capacity of carbon-foams: grand canonical Monte Carlo simulations. J Phys Chem C 115:2476–2482. doi:10.1021/jp104889a
5. Rafati AA, Hashemianzadeh SM, Nojini ZB, Naghshineh N (2010) Canonical Monte Carlo simulation of adsorption of O_2 and N_2 mixture on single walled carbon nanotube at different temperatures and pressures. J Comput Chem 31:1443–1449. doi:10.1002/jcc.21428
6. Romanos GE et al (2011) Controlling and quantifying oxygen functionalities on hydrothermally and thermally treated single-wall carbon nanotubes. J Phys Chem C 115:8534–8546. doi:10.1021/jp200464d
7. Maiti A (2011) Energetic stability of hydrogen-chemisorbed carbon nanotube structures. Chem Phys Lett 508:107–110. doi:10.1016/j.cplett.2011.04.020
8. Rashidi AM, Nouralishahi A, Khodadadi AA, Mortazavi Y, Karimi A, Kashefi K (2010) Modification of single wall carbon nanotubes (SWNT) for hydrogen storage. Int J Hydrogen Energ 35:9489–9495. doi:10.1016/j.ijhydene.2010.03.038
9. Karatepe N, Yuca N (2011) Hydrogen adsorption on carbon nanotubes purified by different methods. Int J Hydrogen Energ 36:11467–11473
10. Biswas MM, Cagin T (2010) Simulation studies on hydrogen sorption and its thermodynamics in covalently linked carbon nanotube scaffold. J Phys Chem B 114:13752–13763. doi:10.1021/jp1027806
11. Xiao H, Li SH, Cao JX (2009) First-principles study of Pd-decorated carbon nanotube for hydrogen storage. Chem Phys Lett 483:111–114. doi:10.1016/j.cplett.2009.10.047
12. Cheng J, Zhang L, Ding R, Ding Z, Wang X, Wang Z (2007) Grand canonical Monte Carlo simulation of hydrogen physisorption in single-walled boron nitride nanotubes. Int J Hydrogen Energ 32:3402–3405. doi:10.1016/j.ijhydene.2007.02.037
13. Xiu-Ying L, Chao-Yang W, Yong-Jian T, Wei-Guo S, Wei-Dong W, Jia-Jing X (2009) Theoretical studies on hydrogen adsorption of single-walled boron-nitride and carbon nanotubes using grand canonical Monte Carlo method. Physica B 404:1892–1896. doi:10.1016/j.physb.2008.11.073
14. Cheng J, Ding R, Liu Y, Ding Z, Zhang L (2007) Computer simulation of hydrogen physisorption in single-walled boron nitride nanotube arrays. Comput Mater Sci 40:341–344. doi:10.1016/j.commatsci.2007.01.006
15. Kowalczyk P, Brualla L, Żywociński A, Bhatia SK (2007) Single-walled carbon nanotubes: efficient nanomaterials for separation and on-board vehicle storage of hydrogen and methane mixture at room temperature? J Phys Chem C 111:5250–5257. doi:10.1021/jp068484u
16. Shadman M, Ahadi Z (2011) Argon and neon storage in single-wall boron nitride nanotubes: a grand canonical Monte Carlo Study. Fuller Nanotub Carbon Nanostruct 19:700–712. doi:10.1080/1536383X.2010.515761
17. Gupta A, Chempath S, Sanborn MJ, Clark LA, Snurr RQ (2003) Object-oriented programming paradigms for molecular modeling. Mol Simul 29:29–46. doi:10.1080/0892702031000065719
18. Frenkel D, Smit B (2001) Understanding molecular simulation: from algorithms to applications. Academic, Orlando
19. Walton KS et al (2008) Understanding inflections and steps in carbon dioxide adsorption isotherms in metal–organic frameworks. J Am Chem Soc 130:406–407. doi:10.1021/ja076595g
20. Bae YS et al (2008) Separation of CO_2 from CH_4 using mixed-ligand metal–organic frameworks. Langmuir 24:8592–8598. doi:10.1021/la800555x
21. Bae YS, Farha OK, Spokoyny AM, Mikrin CA, Hupp JT, Snurr RQ (2008) Carborane-based metal-organic frameworks as highly selective sorbents for CO_2 over methane. Chem Commun 35:4135–4137. doi:10.1039/B805785K